SCIENCE CHINA
Chemistry

•COMMUNICATIONS•

February 2023 Vol.66 No.2: 436–442
https://doi.org/10.1007/s11426-022-1473-5

Precise fabrication of ternary ordered covalent organic frameworks for photocatalysis

Kailong Qian[†], Xinyu Guan[†], Nana Sun & Hai-Long Jiang[*]

Department of Chemistry, University of Science and Technology of China, Hefei 230026, China

Received October 11, 2022; accepted November 26, 2022; published online January 10, 2023

Despite the great success in the synthesis of binary covalent organic frameworks (COFs) in the past decade, the fabrication of structurally ordered ternary COFs remains a big challenge, due to the inevitable competition and exchange of monomers. Herein, two ternary ordered COFs (**2Me-OMe-COF** and **Me-2OMe-COF**) are successfully synthesized by two-step polymerization based on irreversible covalent bonds. In contrast to the ternary random COFs synthesized by one-pot method, ternary ordered COFs possess definite structures at the molecular level. Accordingly, we systematically compare the performance of the two ternary ordered COFs in photocatalytic H_2 production with two corresponding binary COFs as controlled comparison. Significantly, they exhibit very different photocatalytic performance, highlighting the importance of component and structural order for their properties. This work provides a unique strategy to the targeted polymerization and synthesis of ternary ordered, or even multivariate ordered COFs.

covalent organic frameworks, precise fabrication, ordered structure, photocatalysis

Citation: Qian K, Guan X, Sun N, Jiang HL. Precise fabrication of ternary ordered covalent organic frameworks for photocatalysis. *Sci China Chem*, 2023, 66: 436–442, https://doi.org/10.1007/s11426-022-1473-5

Covalent organic frameworks (COFs) featuring crystalline porous structures are composed of multiple organic building units through reversible or irreversible covalent bonds [1]. Possessing high tunability and long-range order in extended two-dimensional (2D) and three-dimensional (3D) structures, COFs show fascinating potential in heterogeneous catalysis [2], gas adsorption and separation [3], energy storage [4], sensing [5], optoelectronics [6], and others. To date, hundreds of COF structures have been reported, in which most of classical COFs are generated with only two monomers. The construction of ternary, or even multivariate COFs is considered as an effect strategy to improve their structural diversity for diverse applications [7]. Unfortunately, the complexity of the reaction will be greatly increased during the one-pot synthesis of ternary COFs. Once the third component is introduced, two isomeric monomers, following the principle of dynamic covalent chemistry (DCC), may undergo exchange reactions as well as inherent competition reactions (Scheme 1a) [8]. As a result, the random distribution will happen for isomeric monomers in ternary COFs, which will result in the destruction of translational symmetry in crystallography and give rise to the transformable local structures. Nevertheless, the structure clarity is vital for studying structure-function relationship, and these random structures will undoubtedly impede further function studies. Therefore, synthesizing ternary ordered COFs with definite structures is of great importance yet remains a grand challenge.

It is assumed that a two-step synthesis strategy might be feasible to ordered ternary COFs, in which the binary oligomers constructed with irreversible covalent bonds, eliminating the above possible competitive and exchange reactions, are pre-isolated, followed by their interconnection

†These authors contributed equally to this work.
*Corresponding author (email: jianglab@ustc.edu.cn)

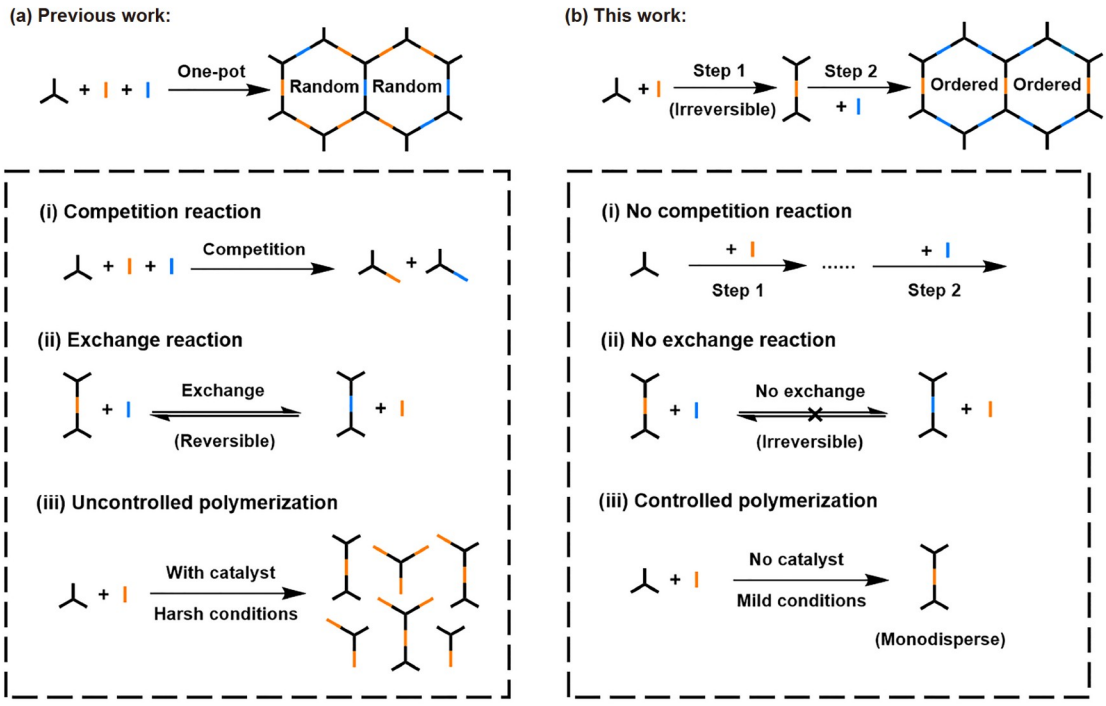

Scheme 1 (a) Reported one-step synthesis of ternary random COFs that might be formed by the corresponding reaction mechanisms; (b) our strategy to the synthesis of ternary ordered COFs and the corresponding characteristics of the reaction (color online).

with the third monomer to afford the resulting ternary COFs (Scheme 1b). Based on the above analysis, covalent connection with high stability and low reversibility is essential for the polymerization reaction to avoid the possible exchange reaction. Especially, the key point of this two-step synthesis lies on the successful preparation of the robust oligomers.

In this work, two novel monodisperse oligomers (**2Tp-OMe** and **2Tp-Me**), which demonstrate high stability under classical solvothermal conditions of COF synthesis, are prepared through controllable condensation of 2,4,6-triformylphloroglucinol (**Tp**) with corresponding linear amino-monomers. Subsequently, the monodisperse oligomers as building blocks are allowed to further copolymerize with the other linear amino-monomer to afford two ternary ordered COFs (**2Me-OMe-COF** and **Me-2OMe-COF**). For comparison, two corresponding binary ordered COFs (**3Me-COF** and **3OMe-COF**) are also prepared. Meanwhile, exchange experiments for both monodisperse oligomers and COFs are conducted and demonstrate a very low degree of reversibility, demonstrating the negligible exchange reactions. Finally, the four ordered COFs are comprehensively characterized and evaluated for photocatalytic H_2 production, in which **2Me-OMe-COF** exhibits the highest photocatalytic activity.

Encouraged by previous work declaring enol-imine will undergo irreversible proton migration to form the exceptionally stable keto-enamine structures, β-ketoenamine bonds are selected as the linkages based on **Tp** [9]. Two linear amino-monomers 4,4′-diamino-3,3′-dimethylbiphenyl (**Me**) and 4,4′-diamino-3,3′-dimethoxybiphenyl (**OMe**) are employed to synthesize the oligomers and COFs. Unfortunately, traditional one-pot methods could only produce ternary random COFs with four possible secondary building units (SBUs: **3Me-SBU**, **2Me-OMe-SBU**, **Me-2OMe-SBU** and **3OMe-SBU**) coexisting in a single framework (Figure 1a). To solve this problem, a two-step method is developed. Firstly, two oligomers (**2Tp-Me** and **2Tp-OMe)** are prepared in tetrahydrofuran at room temperature by pre-condensation of **Tp** with **Me** (or **OMe**). Subsequently, the two ternary ordered COFs (**2Me-OMe-COF** and **Me-2OMe-COF)** are prepared by polymerizing **2Tp-OMe** with **Me**, and **2Tp-Me** with **OMe** respectively, using *o*-dichlorobenzene as the solvent under solvothermal conditions for three days. For comparison, two binary COFs (**3Me-COF** and **3OMe-COF**) are synthesized under similar solvothermal conditions by polymerizing **Tp** with **Me** and **OMe**, respectively (Figure 1b). Notably, each ordered COF has only one corresponding SBU in its single framework.

As noted above, the preparation of monodispersed oligomers (**2Tp-Me** and **2Tp-OMe**) is the key step in the synthesis of ternary ordered COFs, and nuclear magnetic resonance (NMR) spectra are employed for structural determination of these key intermediates. Actually, the oligomers pose large challenges for separation and characterization due to the insolubility in traditional organic solvents,

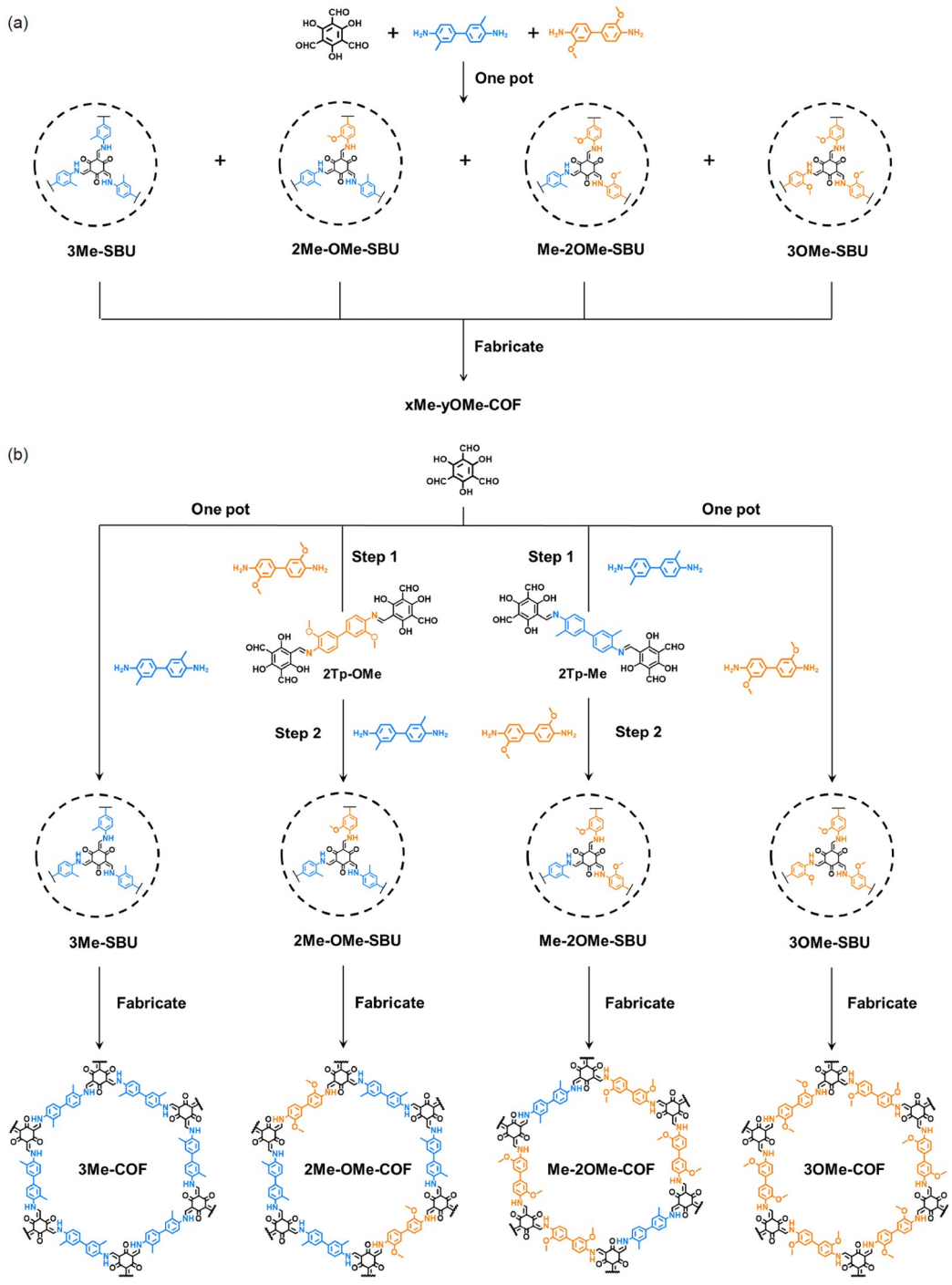

Figure 1 Synthesis and structures of (a) ternary random COFs possibly involving mixed SBUs by one-pot synthesis, (b) ternary ordered COFs (**2Me-OMe-COF** and **Me-2OMe-COF**) by two-step synthesis and binary ordered COFs (**3Me-COF** and **3OMe-COF**), in which single SBU is involved in each COF skeleton (color online).

and D_2SO_4 is therefore adopted as the deuterium reagent. The ^{1}H NMR spectra of both **2Tp-OMe** and **2Tp-Me** clearly show the ratio of aldehyde groups to imine bonds and methyl/methoxy groups as 2:1:1, which is consistent with our proposed compositions (Figures S1 and S2, Supporting Information online). Given that it is difficult to observe the signals of active hydrogen of hydroxyl groups due to rapid H-D exchange in the strong acid, some other NMR spectra are collected. As shown in ^{13}C NMR, the signals of the characteristic carbon can be clearly assigned (190 ppm for the aldehyde groups, 13 ppm for the methyl groups and 53 ppm for the methoxy groups), and it is surprising that there are only imine signals (~150 ppm) instead of carbonyl signals (~182 ppm) assigned to keto-enamine. This indicates

that no transformation from enol-imine to keto-enamine occurs and only one amino group reacts with each **Tp** moiety (Figures S3 and S4). Heteronuclear singular quantum correlation (HSQC) spectra that can provide information of the direct connection between ^{13}C and ^{1}H have been used for further identification. Strong coupling correlations are observed between the corresponding ^{1}H and ^{13}C of methyl/methoxy groups, substituted benzene and imine bonds except for the aldehyde groups, which may be caused by strong hydrogen bond interactions (Figures S5 and S6). To determine the coupling signals of aldehyde groups, hydrogen and heteronuclear multiple bond correlation (HMBC) spectrum as a powerful tool for detecting multiple-bond coupling signals of ^{13}C-^{1}H has been measured. Apparently, the ^{1}H signals (~9.8 ppm) of the aldehyde groups are strongly coupled with the ^{13}C signals (~171, ~170 and ~96 ppm) of **Tp** units, which indicates that the ^{1}H signals (~9.8 ppm) belong to the aldehyde group (Figures S7 and S8). In addition, matrix-assisted laser desorption/ionization time-of-flight (MALDI-TOF) mass spectra of both oligomers unambiguously demonstrates the formation of monodisperse fragment instead of a mixture (Figure 2).

Potential exchange reaction between isomeric monomers is another potential factor that leads to the loss of structural order of ternary COFs. To determine the degree of reversibility in the reaction of COF synthesis, exchange experiments are carried out for both oligomers and COFs under the similar solvothermal conditions of COF synthesis. Oligomer exchange experiments are attempted between **2Tp-Me**, **2Tp-OMe** and the corresponding mono-functional amines. The exchanged products **Tp-3OMe** and **Tp-3Me** are quantified in ^{1}H NMR with *o*-dichlorobenzene as internal standards. The exchange amount in the reaction can be calculated based on the ratio of the exchanged products to the initial oligomers (Figures S11). As displayed in ^{1}H NMR spectra (Figures S12 and S14), no obvious exchange (< 3%) can be observed with the addition of equivalent competitive amino-monomers. Even with excessive mono-functional amines, the exchange amount (< 7%) is still limited (Figures S13 and S15). Furthermore, solid-state ^{13}C NMR spectra have been adopted to evaluate the exchange amount between monomers and COFs, which confirms the negligible exchange after the reaction (Figure S16).

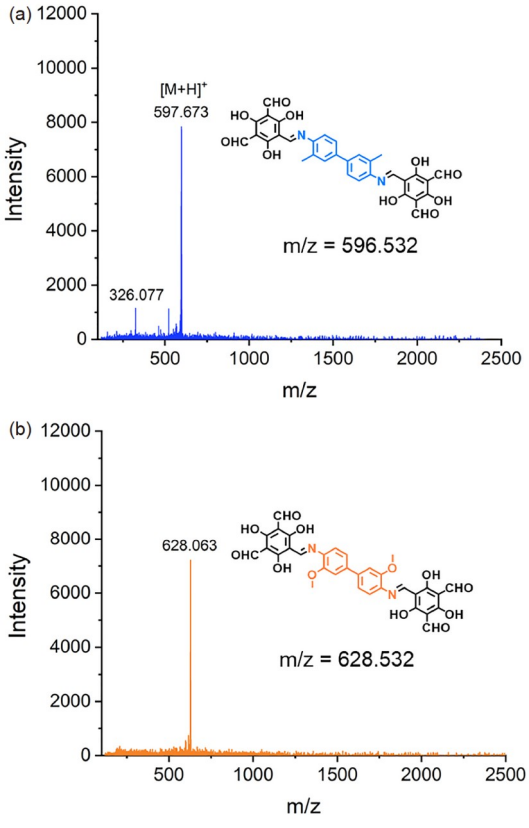

Figure 2 MALDI-TOF mass spectra for the (a) **2Tp-Me** and (b) **2Tp-OMe** oligomers (color online).

The crystal structures of the as-prepared COFs are determined by powder X-ray diffraction (PXRD) patterns. The lattices of the two binary COFs are assumed to be close to hexagonal space group *P*6/*m* ($a = b$, $\alpha = \beta = 90°$, $\gamma = 120°$) (Figures S17 and S18), which is reduced to be *P*2/*m* ($\alpha = \beta = 90°$) for ternary COFs due to the breaking of C_3 symmetry in SBUs (Figures S19 and S20). All COFs have nearly identical diffraction patterns according to their similar crystal structures, with diffraction peaks at 2θ = 3.5°, 6.2°, 7.1°, and 26.5° assigned to the (100), (110), (200) and (001) facets, respectively (Figure 3a, d). Pawley refinement results are in good agreement with the experimental data with low R_{wp} and R_p values, indicating the high crystallinity of the four COFs.

Nitrogen adsorption tests at 77 K for pore structure determination exhibit the Brunauer-Emmett-Teller (BET) surface areas of 754, 746, 707 and 656 $m^2 g^{-1}$ for **3Me-COF**, **2Me-OMe-COF**, **Me-2OMe-COF** and **3OMe-COF**, respectively (Figure 3e–h), and pore size distributions show very small differences among the four COFs in the range from 1 to 1.5 nm (Figure S21). Fourier-transform infrared (FT-IR) spectra of the four COFs display the C–N stretching around 1,268 cm^{-1} as the characteristic absorption of β-ketoenamine. The strong peaks at 1,617 cm^{-1} (C=O) and 1,578 cm^{-1} (C=C) assigned to the keto form also support the successful synthesis of COFs (Figure S22a). Solid-state ^{13}C NMR spectra are also obtained to confirm the intrinsic structure of COFs. Specifically, the typical signals at 15.7 and 54.8 ppm, which are assignable to methyl and methoxy groups based on the previous report [10], are observed for both **2Me-OMe-COF** and **Me-2OMe-COF**, while the ratios of their integral areas are approximately 2:1 and 1:2, in line with the expected structures (Figure 4). In addition, the morphologies of all COFs are spherical with diameters of 1–2 μm, as revealed by scanning electron microscopy (SEM) observation (Figure S23).

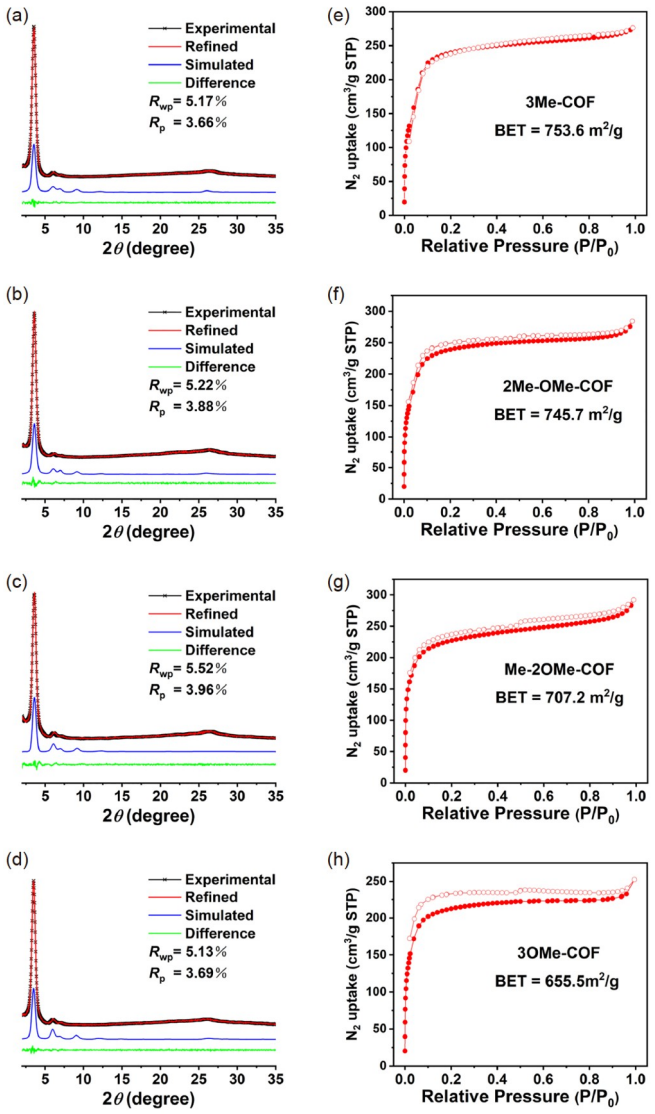

Figure 3 Experimental, refined, and simulated PXRD patterns of **3Me-COF** (a), **2Me-OMe-COF** (b), **Me-2OMe-COF** (c), and **3OMe-COF** (d). Nitrogen sorption isotherms of **3Me-COF** (e), **2Me-OMe-COF** (f), **Me-2OMe-COF** (g) and (h) **3OMe-COF** (color online).

Various spectroscopic and electrochemical experiments have been further performed to investigate the photoelectric properties of these COFs. Ultraviolet-visible (UV-vis) diffuse reflectance spectra unveil that these β-keto-enamine-linked COFs have excellent light absorption between 200 to 600 nm with almost the same band gaps (1.7–1.8 eV) acquired by Tauc plots of the Kubelka-Munk function (Figure S24). Notably, with the increase in the proportion of methoxy groups in COFs, the absorption wavelength has a tendency to redshift and the bandwidth gradually become narrower due to the effect of auxochromes. The conduction bands (CBs) of COFs are estimated by Mott-Schottky measurements with frequencies of 1,000, 1,500, and 2,000 Hz in 0.1 M Na_2SO_4 aqueous solution (pH 6.8). The flat band potential can be evaluated from its intersection with the *x*-axis, with values of −0.95, −1.04, −1.06 and −1.11 V *vs*. normal hydrogen electrode (NHE) for **3Me-COF**, **2Me-OMe-COF**, **Me-2OMe-COF** and **3OMe-COF**, respectively (Figure S25). According to the above results, it is able to determine the band positions for the four COFs (Figure 5a). The photoluminescence (PL) spectrum of **3Me-COF** shows an obvious fluorescence emission at 580 nm under excitation at 440 nm, which decreases gradually with the increased density of methoxy groups and almost cannot be observed for **3OMe-COF**, suggesting the better intramolecular charge separation capability of **3OMe-COF** (Figure S26). In general, methoxy groups as stronger electron donors due to the p-π conjugation effect directly influence the photoelectric properties of COFs and illustrate these differences.

Given that well defined and ordered COF structures can provide in-depth insights into structure-activity relationships, we set out to investigate the photocatalytic H_2 production performance of the four ordered COFs under visible-light irradiation (λ > 380 nm). Surprisingly, all four photocatalysts exhibit outstanding activity (27.6 mmol g^{-1} h^{-1} for **3Me-COF**, 33.1 mmol g^{-1} h^{-1} for **2Me-OMe-COF**, 19.5 mmol g^{-1} h^{-1} for **Me-2OMe-COF** and 10.1 mmol g^{-1} h^{-1} for **3OMe-COF**) in the H_2 production with Pt nanoparticles as cocatalysts (Figure 5b), superior to most COF-based photocatalysts. Moreover, photocurrent response and electrochemical impedance spectroscopy (EIS) demonstrate the superior charge separation and conductivity of **2Me-OMe-COF** (Figure 5c, d), which is consistent with the optimized photocatalytic performance. To further understand the reasons behind the differences in the photocatalytic activities, the stability of these COFs is evaluated. Unexpectedly, only **3Me-COF** exhibited well maintained crystallinity after reaction based on powder XRD results, demonstrating discriminated stability for the four COFs (Figure S27). The stability of COFs is proved by XRD patterns after being soaked in different solvents, with **2Me-OMe-COF** as the representative (Figure S28). Moreover, the negligibly changed FT-IR spectra and solid-state ^{13}C NMR spectra before and after the photocatalytic reaction can further imply the preserved chemical structures after photocatalysis (Figures S29 and S30). As a result, although **3OMe-COF** has the best charge separation efficiency, the poor stability of its structure greatly restricts its photocatalytic performance. For **2Me-OMe-COF**, the highest activity may be attributed to the balance between the moderately high stability and good charge separation ability, which indicates that the final H_2 production activity is determined by the balanced effect based on various factors [11].

In summary, we develop an effective synthetic strategy to ternary ordered COFs *via* a two-step controllable polymerization based on irreversible bonds. This two-step

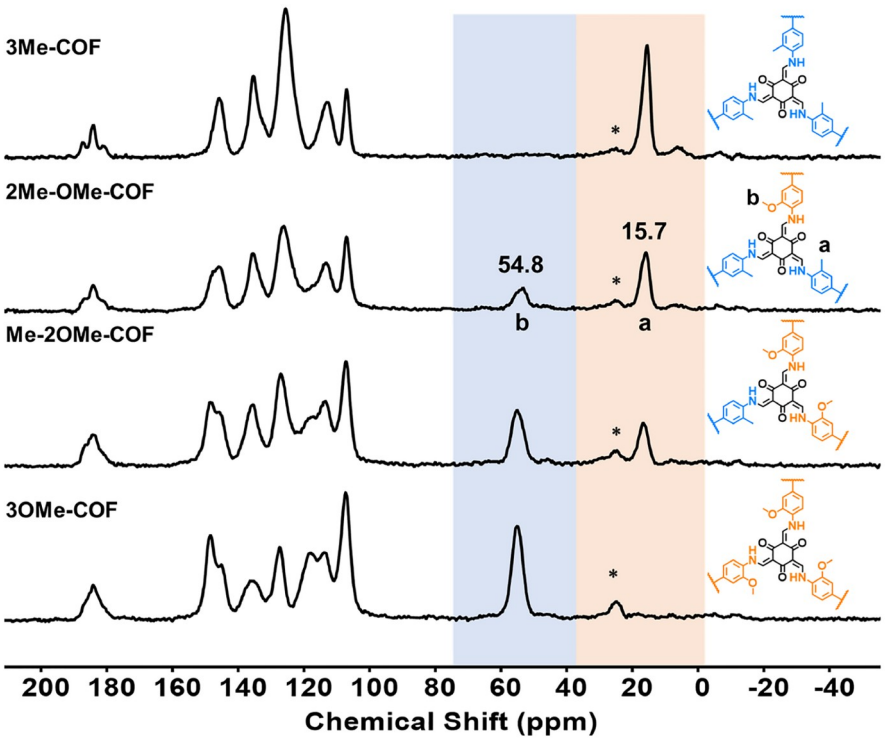

Figure 4 Solid-state ^{13}C NMR spectra of **3Me-COF**, **2Me-OMe-COF**, **Me-2OMe-COF** and **3OMe-COF** (color online).

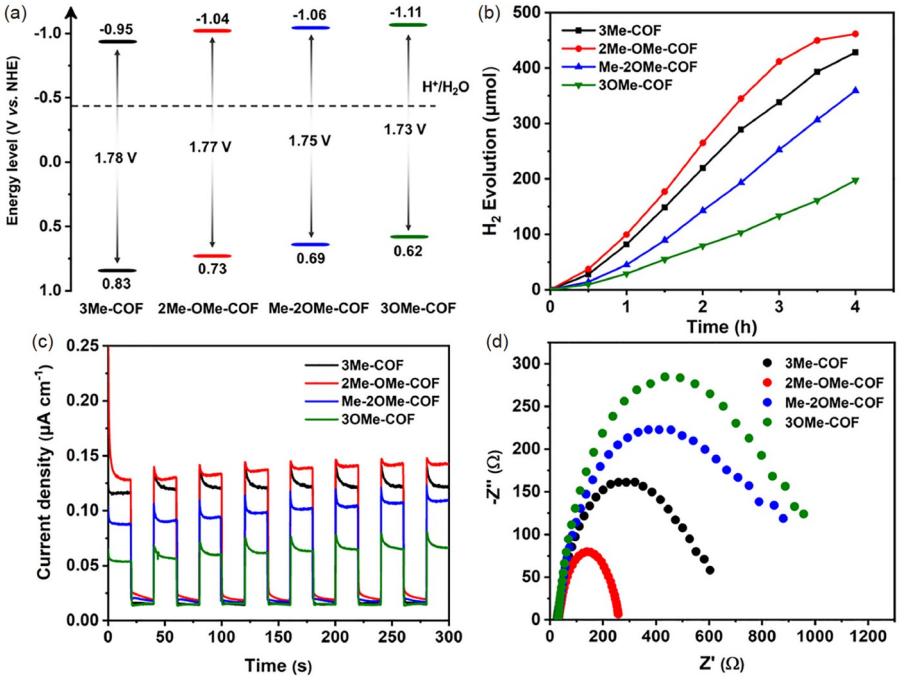

Figure 5 (a) Band alignment maps, (b) photocatalytic H_2 production, (c) photocurrent response, and (d) EIS Nyquist plots for **3Me-COF**, **2Me-OMe-COF**, **Me-2OMe-COF** and **3OMe-COF** (color online).

strategy succeeds in the construction of ternary ordered COFs, which will significantly extend the structure diversity and application fields of COFs. More importantly, the multivariate frameworks with high degree of tunability and highly ordered structures at molecular level will be ideal platforms for in-depth study of the structure-function relationship. This work provides a guideline to produce multivariate COFs with long-range order and well-defined local structures, which are important for precise fabrication, functional tailorability and enhanced performance.

Acknowledgements This work was supported by the National Key Research and Development Program of China (2021YFA1500400), the National Natural Science Foundation of China (21725101, 22205224, 22205225, 22161142001), China Postdoctoral Science Foundation (BX2021281, 2021M703064), and the Fundamental Research Funds for the Central Universities (WK3450000007, WK2060000038, WK2060000041, WK2060000045).

Conflict of interest The authors declare no conflict of interest.

Supporting information The supporting information is available online at chem.scichina.com and link.springer.com/journal/11426. The supporting materials are published as submitted, without typesetting or editing. The responsibility for scientific accuracy and content remains entirely with the authors.

1 (a) Coté AP, Benin AI, Ockwig NW, O'Keeffe M, Matzger AJ, Yaghi OM. *Science*, 2005, 310: 1166–1170; (b) Ding SY, Wang W. *Chem Soc Rev*, 2013, 42: 548–568; (c) Geng K, He T, Liu R, Dalapati S, Tan KT, Li Z, Tao S, Gong Y, Jiang Q, Jiang D. *Chem Rev*, 2020, 120: 8814–8933; (d) Zhou ZB, Han XH, Qi QY, Gan SX, Ma DL, Zhao X. *J Am Chem Soc*, 2022, 144: 1138–1143; (e) Guan X, Li H, Ma Y, Xue M, Fang Q, Yan Y, Valtchev V, Qiu S. *Nat Chem*, 2019, 11: 587–594; (f) Duan H, Li K, Xie M, Chen JM, Zhou HG, Wu X, Ning GH, Cooper AI, Li D. *J Am Chem Soc*, 2021, 143: 19446–19453

2 (a) Ding SY, Gao J, Wang Q, Zhang Y, Song WG, Su CY, Wang W. *J Am Chem Soc*, 2011, 133: 19816–19822; (b) Vyas VS, Haase F, Stegbauer L, Savasci G, Podjaski F, Ochsenfeld C, Lotsch BV. *Nat Commun*, 2015, 6: 8508; (c) Wang H, Qian C, Liu J, Zeng Y, Wang D, Zhou W, Gu L, Wu H, Liu G, Zhao Y. *J Am Chem Soc*, 2020, 142: 4862–4871; (d) Wang X, Han X, Zhang J, Wu X, Liu Y, Cui Y. *J Am Chem Soc*, 2016, 138: 12332–12335; (e) Yan S, Guan X, Li H, Li D, Xue M, Yan Y, Valtchev V, Qiu S, Fang Q. *J Am Chem Soc*, 2019, 141: 2920–2924; (f) Qian Y, Li D, Han Y, Jiang HL. *J Am Chem Soc*, 2020, 142: 20763–20771; (g) Xu H, Gao J, Jiang D. *Nat Chem*, 2015, 7: 905–912; (h) Gong YN, Zhong W, Li Y, Qiu Y, Zheng L, Jiang J, Jiang HL. *J Am Chem Soc*, 2020, 142: 16723–16731; (i) Gong Y, Guan X, Jiang HL. *Coord Chem Rev*, 2023, 475: 214889; (j) Lu M, Zhang M, Liu J, Yu TY, Chang JN, Shang LJ, Li SL, Lan YQ. *J Am Chem Soc*, 2022, 144: 1861–1871

3 (a) Han SS, Furukawa H, Yaghi OM, Goddard III WA. *J Am Chem Soc*, 2008, 130: 11580–11581; (b) Furukawa H, Yaghi OM. *J Am Chem Soc*, 2009, 131: 8875–8883

4 (a) DeBlase CR, Silberstein KE, Truong TT, Abruña HD, Dichtel WR. *J Am Chem Soc*, 2013, 135: 16821–16824; (b) Li J, Jing X, Li Q, Li S, Gao X, Feng X, Wang B. *Chem Soc Rev*, 2020, 49: 3565–3604; (c) Vitaku E, Gannett CN, Carpenter KL, Shen L, Abruña HD, Dichtel WR. *J Am Chem Soc*, 2020, 142: 16–20

5 (a) Meng Z, Mirica KA. *Chem Soc Rev*, 2021, 50: 13498–13558; (b) Wu X, Han X, Xu Q, Liu Y, Yuan C, Yang S, Liu Y, Jiang J, Cui Y. *J Am Chem Soc*, 2019, 141: 7081–7089

6 Keller N, Bein T. *Chem Soc Rev*, 2021, 50: 1813–1845

7 (a) Xu H, Gao J, Jiang D. *Nat Chem*, 2015, 7: 905–912; (b) Sun Q, Tang Y, Aguila B, Wang S, Xiao F-, Thallapally PK, Al-Enizi AM, Nafady A, Ma S. *Angew Chem Int Ed*, 2019, 58: 8670–8675; (c) Li RL, Yang A, Flanders NC, Yeung MT, Sheppard DT, Dichtel WR. *J Am Chem Soc*, 2021, 143: 7081–7087; (d) Dong B, Wang L, Zhao S, Ge R, Song X, Wang Y, Gao Y. *Chem Commun*, 2016, 52: 7082–7085; (e) Yang Y, Faheem M, Wang L, Meng Q, Sha H, Yang N, Yuan Y, Zhu G. *ACS Cent Sci*, 2018, 4: 748–754; (f) Zhou T, Huang X, Mi Z, Zhu Y, Wang R, Wang C, Guo J. *Polym Chem*, 2021, 12: 3250–3256; (g) Jin Y, Hu Y, Zhang W. *Nat Rev Chem*, 2017, 1: 0056; (h) Crowe JW, Baldwin LA, McGrier PL. *J Am Chem Soc*, 2016, 138: 10120–10123; (i) Pang ZF, Xu SQ, Zhou TY, Liang RR, Zhan TG, Zhao X. *J Am Chem Soc*, 2016, 138: 4710–4713

8 (a) Qian C, Qi QY, Jiang GF, Cui FZ, Tian Y, Zhao X. *J Am Chem Soc*, 2017, 139: 6736–6743; (b) Zhan G, Cai ZF, Martínez-Abadía M, Mateo-Alonso A, De Feyter S. *J Am Chem Soc*, 2020, 142: 5964–5968

9 Kandambeth S, Mallick A, Lukose B, Mane MV, Heine T, Banerjee R. *J Am Chem Soc*, 2012, 134: 19524–19527

10 Chandra S, Kandambeth S, Biswal BP, Lukose B, Kunjir SM, Chaudhary M, Babarao R, Heine T, Banerjee R. *J Am Chem Soc*, 2013, 135: 17853–17861

11 Bai Y, Wilbraham L, Slater BJ, Zwijnenburg MA, Sprick RS, Cooper AI. *J Am Chem Soc*, 2019, 141: 9063–9071